Towards low-cost, high-sensitivity point-of-care diagnostics using VCO-based ESR-on-a-chip detectors

Benedikt Schlecker[1,2], *Student Member, IEEE,* Alexander Hoffmann[2], Anh Chu[1], *Student Member, IEEE,* Maurits Ortmanns[2], *Senior Member, IEEE,* Klaus Lips[3], and Jens Anders[1], *Senior Member, IEEE*

***Abstract*—In this paper, we present a new architecture for VCO-based ESR detection for a future use in portable, point-of-care ESR spectrometers. The proposed architecture is centered around an ASIC containing a VCO-based ESR detector with two distinct tuning ports with largely different VCO gains to enable wide frequency sweeps and small-signal frequency modulations while keeping the requirements on the digital-to-analog converter driving the ports manageable. Furthermore, in order to avoid the very small output referred frequency noise levels associated with frequency dividers, which would place stringent requirement on the subsequent frequency demodulation block, the proposed ASIC features a second VCO for an on-chip frequency downconversion via mixing. To allow for a precise derivation of the operating frequency from an external reference as it is required for quantitative ESR experiments, all on-chip VCOs are embedded into phase locked loops. The proposed architecture is verified with ESR experiments on commonly used ESR standard samples (DPPH and BDPA). In these experiments, a state-of-the-art sensitivity of $1.7 \times 10^9\,\mathrm{spins}/(\mathrm{G}\sqrt{\mathrm{Hz}})$ was achieved using a back-end signal processing on a low-cost FPGA. The presented proof-of-principle experiment clearly demonstrate the potential of the proposed VCO-based ESR detection system for future point-of-care applications.**

***Index Terms*—Electron spin resonance (ESR), spectroscopy, magnetic sensors, resonant sensors, voltage-controlled oscillators (VCO), point-of-care (PoC).**

I. Introduction

THANKS to recent advances in microwave electronics, electron spin resonance (ESR) spectroscopy is gaining increasing attention in both life science and materials science applications, because the electron spin can serve as a nanoscopic probe of its environment inside a sample with very high specificity. Example emerging fields for ESR include in-cell ESR experiments to study cells under biologically relevant conditions [1], [2] and the in-vivo/in-vitro detection of free radicals. These free-radicals play a major role in many diseases and can also directly be related to premature cell aging [3], [4]. Moreover, paramagnetic defects in semiconductor and organic materials are also ESR-active, rendering ESR a prime modality for characterizing novel materials and devices [5], [6]. The high specificity of ESR originates from the resonant interaction between the magnetic moment of the electron spin and an applied static magnetic field (B_0-field) illustrated in Fig. 1. For a spin-half particle such as the electron, the interaction with the magnetic field leads to a splitting of the degenerated energy level at $B_0 = 0\,\mathrm{T}$ into two discrete energy levels (Zeemann splitting). Transitions between the two levels can be induced by applying a time-varying magnetic field (B_1-field), whose frequency matches the resonance condition

$$\omega_{B_1} = |\gamma_\mathrm{e} \cdot B_0|, \tag{1}$$

where $\gamma_\mathrm{e} \approx -2\pi \cdot 28\,\mathrm{GHz/T}$ is the electron gyromagnetic ratio and B_0 is the applied static magnetic field, respectively. The excellent specificity of ESR originates from the fact, that minuscule changes in the magnetic and electronic environment of the electron spin, e. g. caused by other electrons or nearby nuclear spins, produce changes in the energy difference between the two states or introduce additional sub energy levels. Therefore, the ESR spectrum is a very specific and thus informative map of the environment of the spin inside the sample. According to the above discussion, ESR spectroscopy bears many similarities with its better-known relative, nuclear magnetic resonance (NMR) spectroscopy, where a nuclear spin is used to read out information about the sample. However, their major differences lie in the achievable limit of detection and the intrinsic applicability of the method: On the one hand, inductively-detected NMR provides a ubiquitously applicable sensing method, which can determine the structure and dynamics of almost any molecule, while ESR suffers from the fact that paramagnetic species are much less prevalent in nature than NMR active nuclei. On the other hand, NMR suffers from an approximately five to seven orders of magnitude poorer sensitivity compared to ESR. Therefore, the two methods are largely complimentary and the availability of both methods inside portable devices is highly desirable in view of potential future applications in personalized medicine and home diagnostics [7].

While there has been tremendous progress towards portable NMR systems by leveraging the miniaturization capabilities of modern integrated circuit technologies [8], the miniaturization of ESR instrumentation is much less advanced. Existing ESR benchtop systems (e. g. EMXnano, Bruker Corporation or MiniScope MS 5000, Magnettech Gesellschaft für Meß- und Steuertechnik mbH) essentially suffer from sizes and weights which prohibit truly portable applications. In this paper, we

This paper is an extended version of the conference proceedings paper presented at the 2017 IEEE Sensors Conference, held in Glasgow, UK on Oct. 30 – Nov. 1 2017.

[1] University of Stuttgart, Institute of Smart Sensors, Stuttgart, Germany
[2] University of Ulm, Institute of Microelectronics, Ulm, Germany
[3] Berlin Joint EPR Lab, Helmholtz Zentrum Berlin für Materialien und Energie, Germany

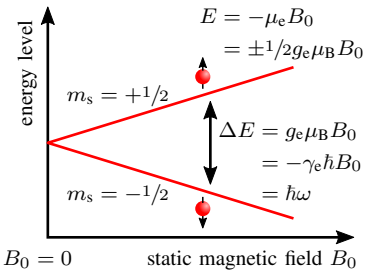

Fig. 1. Illustration of the Zeeman splitting inside a static magnetic field B_0.

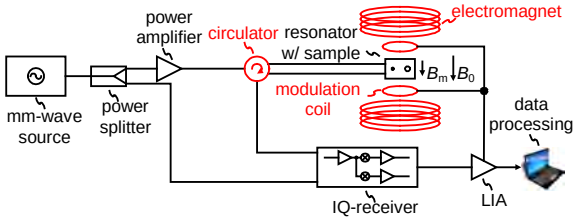

Fig. 2. Conventional setup for continuous-wave ESR experiments.

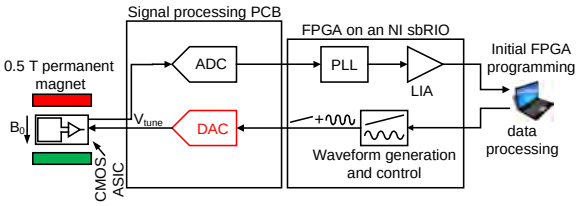

Fig. 3. VCO-based ESR setup similar to [9].

present some recent advances in the use of integrated circuit technology towards portable ESR spectrometers. More specifically, we will present some extensions to the VCO-based ESR-on-a-chip technology introduced by our group in [9], [10], where the paper at hand is an extension of the conference paper [11], presenting a more detailed modelling as well as additional experimental results.

II. ESR Working Principle and Conventional ESR Detection

As illustrated in Fig. 1, the magnetic dipole moment μ_e of a spin associated with an unpaired electron interacts with an externally applied magnetic field B_0, resulting in two (for an isolated electron) distinct energy levels, whose difference grows linearly with B_0 (Zeeman splitting). Transitions between the two energy states can be induced by applying a microwave magnetic field with an appropriate photon energy of $E = \hbar\omega = -\hbar\gamma_e B_0$, where $\hbar$ is the reduced Planck constant and γ_e the gyromagnetic ratio of the electron which for a free electron takes on a value of $\gamma_e \approx -2\pi \cdot 28\,\frac{\mathrm{GHz}}{\mathrm{T}}$. Consequently, for typical magnetic field strengths of benchtop ESR spectrometers between $0.3\,\mathrm{T}$ and $2\,\mathrm{T}$, the required ESR frequencies range from approximately $9\,\mathrm{GHz}$ to $56\,\mathrm{GHz}$. Therefore, compared to NMR techniques, where the values of $\gamma/2\pi$ for common nuclei are in the range of MHz to some tens of MHz, in ESR, the frequencies of interest are significantly higher, rendering both the design of the required detectors and that of the required electronics more challenging. Together with the much shorter relaxation times in ESR compared to NMR experiments (nansoceconds to microseconds range vs. milliseconds to seconds), pulsed experiments as they are routinely performed in NMR spectroscopy, are still very challenging in ESR and require very expensive equipment. As a consequence, most ESR experiments in general and all ESR experiments in the available benchtop ESR spectrometers, are still carried out in the continuous-wave (cw) mode using the setup of Fig. 2. According to the figure, in a conventional cwESR experiment, the sample is contained inside a resonator, which in turn is placed inside a sweepable electromagnet that produces the required B_0-field. An ESR experiment is then performed by irradiating the sample with an RF-magnetic field (B_1-field) of a fixed frequency ω_{B_1} and slowly sweeping the B_0-field through the resonance condition $|\omega_{B_1}| = |\gamma_e| \cdot B_0$. The ESR spectrum is recorded by monitoring the change in reflected power caused by the resonant sample absorption. In order to improve the achievable signal-to-noise ratio (SNR), a lock-in detection scheme is typically applied by modulating the B_0-field strength with typical modulation frequencies in the kilohertz range and modulation amplitudes in the range of a fraction of a Gauss to tens of Gauss ($1\,\mathrm{G} = 100\,\mu\mathrm{T}$). In summary, a conventional cwESR experiment requires a sweepable magnetic field, a (usually mechanically tunable) resonator, a high power microwave source and further expensive RF/microwave components, rendering the design of portable ESR spectrometers using the conventional approach a very challenging task due to the sheer size, weight and cost of the components. As one potential solution to this problem, in [9], [11], our group proposed the use of CMOS-integrated VCO-based ESR detectors. In this paper we extend this concept by architectural and circuit level modifications that facilitate the design of future low-cost, portable ESR spectrometers based on permanent magnets.

III. VCO-based ESR-on-a-chip

In the VCO-based ESR setup shown in Fig. 3 [9], the mechanically tunable resonator of Fig. 2 is replaced by a CMOS LC-tank oscillator and the sample is directly placed on top of its planar tank inductor. In this way, the magnetic field generated by the current in the tank inductance can produce the resonant magnetic field B_1, which induces the ESR transitions. This removes the need for a sweepable magnet because the swept-frequency excitation, which is required to operate at a fixed static magnetic field B_0, can be readily produced by a sawtooth waveform applied to the VCO tuning voltage V_{TUNE}, cf. Fig. 3. Naturally, such a frequency sweep experiment is in principle also possible with the conventional setup of Fig. 2 by using a swept frequency excitation at a fixed B_0-field. However, frequency-swept experiments using the conventional resonator-based approach introduce an intrinsic tradeoff between detection sensitivity (requiring high-Q resonators) and sweep range (requiring low-Q, high bandwidth resonators).

In contrast, in VCO-based frequency sweeps, the tank resonant frequency is intrinsically tuned to the correct excitation frequency. This is because a change in the tuning

voltage V_{TUNE} modifies the effective tank capacitance, which in turn changes the resonance frequency of the LC tank, $\omega_{\mathrm{LC}} = 1/\sqrt{LC}$. Thereby, a new oscillation frequency, ω_{osc}, is produced, which can be approximated by [12]:

$$\omega_{\mathrm{osc}} \approx \omega_{\mathrm{LC}} \left(1 - \frac{(\alpha_{\mathrm{od}} - 1)^2}{16 \cdot Q_{\mathrm{coil}}^2}\right), \tag{2}$$

where α_{od} is the so-called overdrive parameter that indicates how much the tank loss is overcompensated by the negative small signal resistance of the active devices in the VCO of Fig. 4[1], cf. [13], [14], and Q_{coil} is the coil quality factor. Importantly, the oscillation frequency follows the tank resonant frequency, producing a constant excitation (and also detection) sensitivity, even for wide-range frequency sweeps. The sweep range is then essentially only limited by the achievable tuning range of the utilized VCO.

In VCO-based ESR experiments, the spectroscopic information is contained in both the frequency ω_{osc} and amplitude A_{osc} of the oscillation. This can be seen from the model of the interaction between the spin ensemble and the VCO shown in Fig. 4. Here, the spin-oscillator interaction is modeled as an inductive coupling between the tank inductor and the spin ensemble, which – in the steady state as it occurs for cwESR experiments – can be modeled as a damped series LC resonator. Using this approach, the ESR-induced change in oscillation frequency $\Delta\omega_{\mathrm{osc}}$ can be approximated according to:

$$\Delta\omega_{\mathrm{osc}}(V_{\mathrm{TUNE}}) = -\frac{1}{2} \cdot \omega_{\mathrm{osc},0}(V_{\mathrm{TUNE}}) \cdot \frac{\Delta L_{\mathrm{spin}}(V_{\mathrm{TUNE}})}{L_0} \tag{3}$$

where $\omega_{\mathrm{osc},0}$ is the nominal, i. e. in the absence of ESR, oscillation frequency, L_0 is the nominal tank inductance and ΔL_{spin} is the ESR induced change in the tank inductance according to:

$$\Delta L_{\mathrm{spin}}(V_{\mathrm{TUNE}}) = \eta\, \chi'\, L_0, \tag{4a}$$

$$\chi' = \frac{\Delta\omega T_2^2}{1 + \Delta\omega^2\, T_2^2 + \gamma^2 B_1^2 T_1 T_2}\, \chi_0\, \omega_{\mathrm{L}}, \tag{4b}$$

where η is the so-called fill factor, i. e. the fraction of the sensitive volume of the inductor, which is filled with ESR active material, χ_0 is the static electron susceptibility, $\Delta\omega = \omega_{\mathrm{osc}} - \omega_{\mathrm{L}}$, $\omega_{\mathrm{L}} = -\gamma_{\mathrm{e}} \cdot B_0$ being the so-called Larmor frequency, T_1 and T_2 are the longitudinal and transverse spin relaxation times and B_1 is the amplitude of the B_1-field.

Since the ESR information is contained in the oscillation frequency, lock-in amplification for sensitivity enhancement can be introduced by a frequency modulation of the VCO current. According to Fig. 3, the required frequency modulation can be introduced by applying a sinewave of appropriate frequency and amplitude in addition to the DC ramp to the tuning voltage V_{TUNE}. Then, for small frequency modulations,

[1]More precisely, α_{od} is given $\alpha_{\mathrm{od}} = G_{\mathrm{m}}/2G_{\mathrm{t}}$, where G_{m} is the transconductance of a single transistor in the crosscoupled transistor pair and G_{t} is the equivalent parallel tank conductance [13]

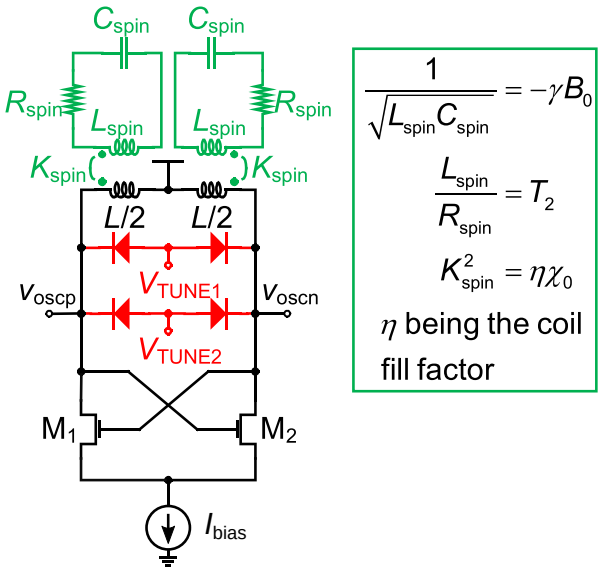

Fig. 4. Schematic of the LC-tank VCO including a model (green) of the interaction between the spin ensemble and the VCO and the relevant model parameters.

the total oscillation frequency in the presence of ESR can be written according to:

$$\omega_{\mathrm{osc}} = \omega_{\mathrm{osc},0}(V_{\mathrm{TUNE,DC}}) + \Delta\omega_{\mathrm{osc}}(V_{\mathrm{TUNE,DC}}) + \frac{\partial\Delta\omega_{\mathrm{osc}}}{\partial V_{\mathrm{TUNE}}}\, \hat{V}_{\mathrm{TUNE}}\, \cos(\omega_{\mathrm{mod}} t) \tag{5}$$

where the partial derivative $\partial\Delta\omega_{\mathrm{osc}}/\partial V_{\mathrm{TUNE}}$ can be obtained from eq. (3), $\hat{V}_{\mathrm{TUNE}}$ is the amplitude of the AC tuning voltage and ω_{mod} is the frequency of the modulation waveform. Eq. (5) clearly describes a frequency modulated signal such that after the PLL-based FM-demodulation block in the architecture of Fig. 3, the ESR information is located at the frequency ω_{mod} from where it can be extracted using a conventional lock-in amplifier.

IV. Design Tradeoffs for VCO-based ESR Detectors

Despite the many advantages of the VCO-based ESR detection approach, there still exist various tradeoffs in the design of the detection ASIC and the overall system. To name a first example, the system presented in [9] used frequency dividers to translate the ESR signal from the ESR frequency around 14 GHz to approximately 220 MHz. Since frequency division affects the center frequency, the ESR-induced frequency shifts and the oscillator's frequency noise in the same way, using this approach, the amplitude of the ESR-signal and the noise floor are reduced by the same division factor. This in turn renders the design of the subsequent (low-noise) FM-demodulator more challenging because it has to meet a more stringent input referred noise specification.

Another tradeoff is associated with the selection of the VCO gain. Here, a large VCO gain maximizes the achievable frequency sweep range, allowing for the detection of wider-range ESR spectra. However, due to the small required frequency deviations (modulation amplitudes between 300 kHz

and $10\,\mathrm{MHz}$ are necessary, which are very small compared to the required DC sweep ranges in the GHz range), large VCO gains make the generation of the frequency modulation via V_{TUNE} harder. As an example, the VCO in [9] was designed with a VCO gain of approximately $1\,\frac{\mathrm{GHz}}{\mathrm{V}}$, resulting in a sweep range which is sufficient to cover all transitions associated with common spin traps used for reactive oxygen species (ROS) detection. However, to generate the small frequency modulation amplitudes for the lock-in detection, this large VCO gain required a DAC capable of producing sinewaves with amplitudes around $300\,\mu\mathrm{V}$, placing a stringent requirement on the DAC dynamic range, which has to be around 16 bit or better to produce both, the required sweep range and the modulation signal. Moreover, voltage noise in the DAC becomes more important as the VCO gain is increased due to the larger AM-to-PM conversion associated with higher gains.

Last but not least, in spectroscopic applications the precise knowledge of the oscillation frequency is of major importance for a classification and evaluation of measured data. In [9] the oscillation frequency was defined by the VCO control voltage V_{TUNE} in an open loop fashion and hence was strongly susceptible to temperature variations of the measurement environment due to the large VCO gain of $1\,\frac{\mathrm{GHz}}{\mathrm{V}}$.

V. VCO-based ESR spectrometer prototype

In the following subsections, improvements to the spectrometer architecture of [9] will be introduced that aim at overcoming the tradeoffs for VCO-based ESR experiments discussed at the end of the previous section.

A. System specifications and overview

The detailed block diagram of the proposed ESR spectrometer is shown in Fig. 5. As a first modification compared to the state-of-the-art, a second on-chip VCO is used to downconvert the ESR signal by means of frequency mixing instead of frequency division, cf. [15], to remove the need for an on-chip frequency divider that would reduce the amplitude of the ESR signal by the division ratio. In [15], this scheme has been applied to fixed frequency oscillator for ESR detection. In this way, the amplitude of the ESR signal is preserved and only its center frequency is shifted, greatly alleviating the burden on the FM-demodulator. Next, the VCO's frequency is controlled by two varactor diodes and therefore two separate tuning voltages. In this way, by designing the varactor diodes for widely different tuning sensitivities, the two contradictory design goals of a large tuning range and at the same time a precise and robust generation of the FM modulation signal can be simultaneously achieved. Finally, all VCOs are embedded into phase-locked loops (PLLs) to precisely derive their oscillation frequency from an external reference, even in the presence of process, voltage and temperature (PVT) variations. More specifically, in order to avoid injection locking between the two on-chip VCOs, they have been embedded into an offset PLL. The offset PLL is implemented by embedding the Q-LO-VCO[2] into a conventional integer-N PLL (sweep PLL in the figure), precisely defining its oscillation frequency from an off-chip reference LO (LO ref in the figure). Since the quadrature LOs (LO I and LO Q in the figure) are phase locked with a 90° phase shift between them, we could use the output of the I mixer to close the offset PLL around the VCO that detects the ESR signal. This offset PLL forces the difference between the LO oscillator and the ESR detector VCO to be equal to the reference frequency of the offset PLL (offset ref in the figure). By choosing this difference frequency sufficiently large, an injection locking between the two on-chip VCOs can be avoided. Here, it should be noted that the tuning input with the large VCO sensitivity of the ESR input is used to close the offset PLL to allow for a maximum sweep range. Also, it should be noted, that the bandwidth of the offset PLL is chosen smaller than the smallest FM modulation frequency for the lock-in detection. In this way, the offset PLL only compensates drifts in the VCO frequency due to temperature but does not effect the ESR-induced change in oscillation frequency. This ESR-induced frequency shift therefore still has to be demodulated by an off-chip FM-demodulator.

An ESR experiment using the architecture of Fig. 5 is conducted by sweeping the reference frequency of the sweep PLL. Then, due to the constant reference frequency for the offset PLL, the LO VCO and the ESR VCO are jointly swept with a constant offset between them. The FM modulation signal is introduced by direct digital synthesis of the required sine wave signal and applying it to the low sensitivity tuning port of the ESR VCO (DDS block in the figure).

In the following sections, we will provide more details of the individual building blocks of the prototype realization.

B. ESR Detector ASIC

The ESR detector ASIC contains all blocks inside the red box in Fig. 5. The ESR VCO features an externally adjustable current biasing. For a bias current of $I_{\mathrm{bias}} = 2.9\,\mathrm{mA}$, which sets the lower limit for a steady oscillation over the whole frequency range, the measured sensitivities of the ESR VCO for the sweep port and the modulation port are $K_{V_{t,1}} = 0.83\,\frac{\mathrm{GHz}}{\mathrm{V}}$ and $K_{V_{t,2}} = 34.4\,\frac{\mathrm{MHz}}{\mathrm{V}}$, respectively. A micrograph of the chip manufactured in a $130\,\mathrm{nm}$ CMOS technology and bonded to our probe head PCB is shown in Fig. 6. To protect the bonding wires, they are covered with epoxy, where care has been taken not to cover the detection coil.

C. Probe head and daughterboard

The detector ASIC is bonded onto a custom probe head PCB (see Fig. 7a) which provides all necessary power supply and control signals for the chip. To perform an ESR experiment with the probe head, first, the sample is placed onto the coil of the ESR VCO and then the ASIC is mounted inside the magnet that generates the B_0 field.

For the off-chip components of the sweep PLL and the offset PLL of Fig. 5, we designed an appropriate daughterboard (see Fig. 7b). Here, the sweep PLL is implemented using the HMC984 (Analog Devices, Inc., Norwood, MA, USA) as phase frequency detector and the offset PLL uses the ADF4002 chip (Analog Devices).

[2]A quadrature LO is not needed for cwESR experiments but can be beneficial for rapid scan ESR experiments; a subject which will be discussed in a follow-up publication.

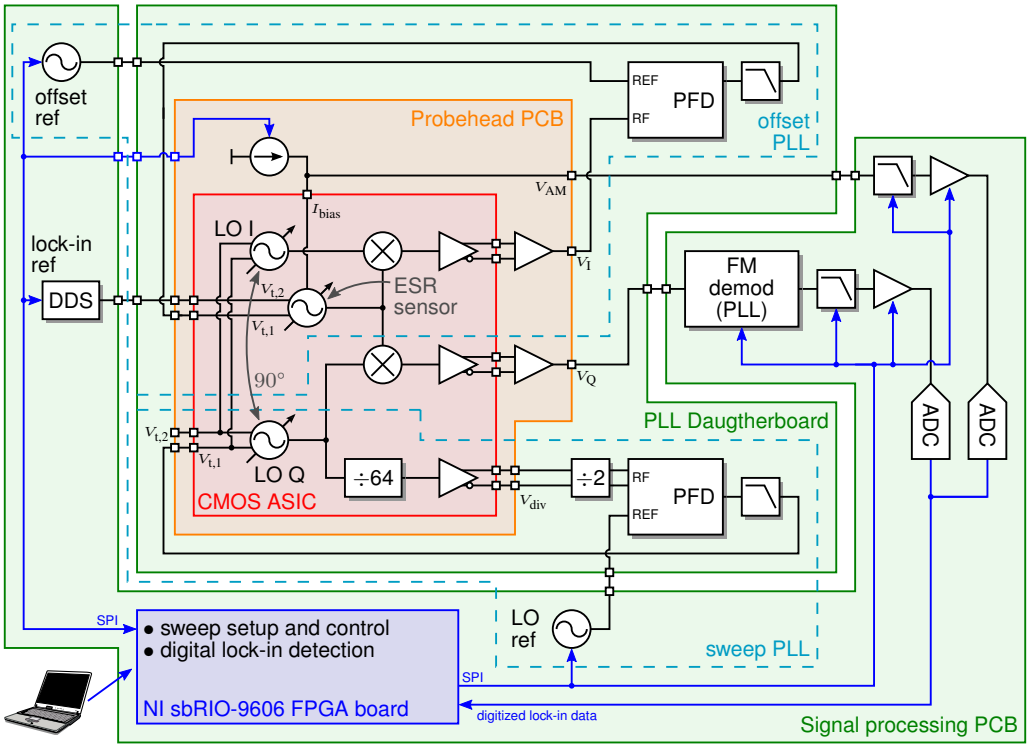

Fig. 5. Detailed block diagram of the proposed ESR spectrometer. The system consist of the CMOS ASIC mounted on the probe head PCB, the PLL daughterboard, the signal processing board and the NI sbRIO-9606 FPGA board. The overall system is controlled by a LabVIEW program running on an external computer.

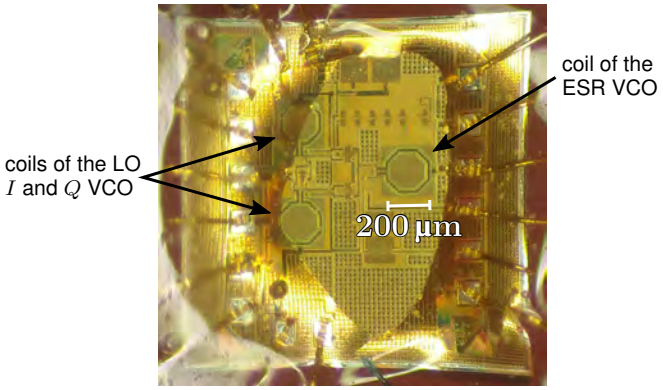

Fig. 6. Micrograph of the presented ESR detection ASIC, bonded to the probe head PCB. The bond wires are protected with epoxy, where the chip surface above the coil of the detection VCO (right octagon) is left open to allow for a sample placement inside the most sensitive detection region.

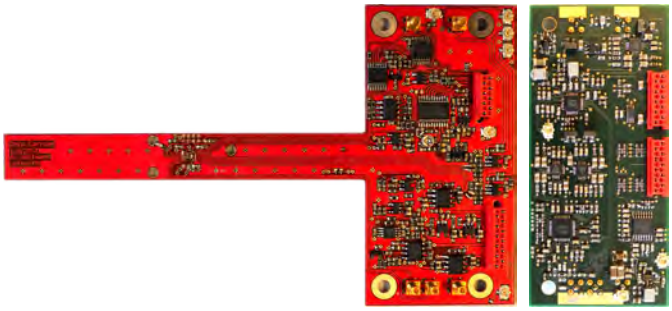

Fig. 7. (a) Probe head PCB with the detection ASIC and (b) daughter board with the corresponding PLLs for the VCO control.

D. Signal processing board

The signal processing board serves as the interface between the analog signals from the probe head board and the digital processing on the FPGA. Furthermore, it provides all control signals for the probe head and the PLL daughterboard. It employs two programmable, fully integrated RF synthesizers (LMX2571, Texas Instruments Inc., Dallas, TX, USA) as frequency references for the sweep and the offset PLL as well as a 14 Bit, 180 MSPS direct digital synthesizer (DDS) (AD9102, Analog Devices) for the generation of the modulation signal for V_{TUNE2} of the detection VCO. In order to prevent destroying the varactor diodes of the detection ASIC, we use a limiting amplifier to drive the tuning voltages that ensures $V_{\mathrm{TUNE2}} > 0.9\,\mathrm{V}$ at all times.

The FM demodulation of the ESR signal is realized by means of a PLL-based demodulator (PFD: ADF4002, Analog Devices, VCO: CVCO55CW-0140-0250, Crystek Corporation®, Fort Myers, FL, USA).

During start-up of the system, a microcontroller (ATmega2560V, Atmel Corporation, San Jose, CA, USA) equipped with a custom firmware ensures that all devices power up in the correct order into a known and stable state. The microcontroller eases and accelerates debugging and electrical tests of the system compared to a full firmware development on the FPGA. After a successful initialization,

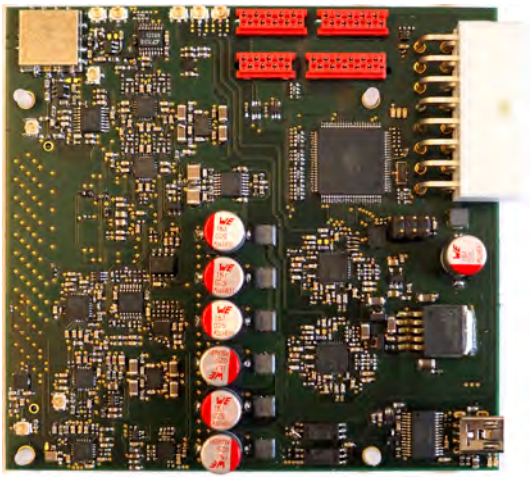

Fig. 8. Custom signal processing board for the interface between the probe head and the FPGA, containing the reference synthesizers, the lock-in reference DDS, the PLL-based FM demodulator and the ADCs for the ESR signal digitalization.

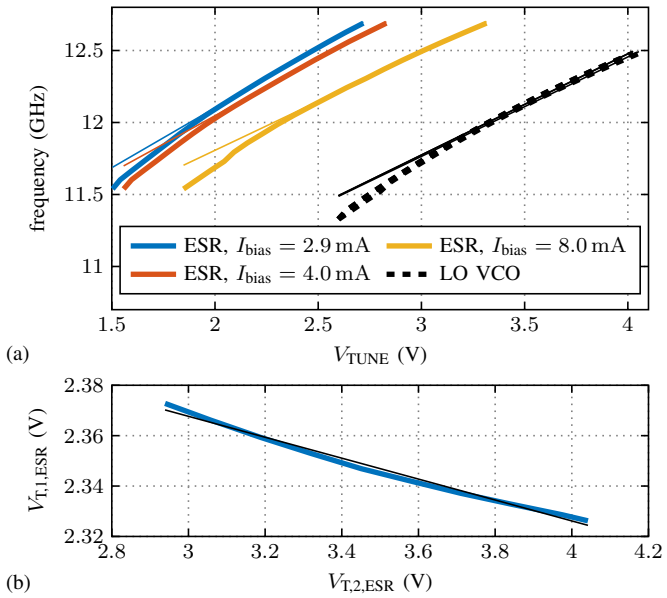

Fig. 9. Tuning characteristics of the detector ASIC. The offset reference frequency is kept constant at 210 MHz. (a): $K_{\text{V,1}}$ of the ESR and LO VCO for different I_{CC} and (b): $K_{\text{V,2,ESR}}$ for $I_{\text{CC}} = 2.9\,\text{mA}$ and $f_{\text{LO}} = 12.22\,\text{GHz}$.

the hardware control for the experiments is handed over to the FPGA board. To avoid interferences due to undesired ground loops, care has been taken during the design of the signal processing board to ensure a galvanic isolation of all interfaces to computers involved in the measurement process. This, together with the possibility of operating the entire system from lithium-ion batteries, minimizes disturbances originating from the power supply line to the system. Fig. 8 shows the assembled signal processing board.

E. FPGA board

The ESR experiments are controlled by a low-cost, embedded real-time computer (sbRIO-9606, National Instruments Corporation, Austin, TX, USA) with an integrated FPGA (Xilinx Spartan-6-LX45). Our signal processing board is connected to the FPGA board via a high-density, high-throughput RMC connector. To orchestrate the ESR experiments, we have developed a program with an easy-to-use GUI in LabVIEW, running on the real-time computer. The program can be executed from any computer via a direct Ethernet connection to the sbRIO.

To perform an ESR experiment, the user has to set the appropriate sweep parameters, such as frequency range, number of measurement points, number of averages, modulation amplitude and frequency, and lock-in time constant. From these parameters the LabVIEW software then determines the corresponding control commands for the individual devices on the signal processing board and the sweep is initialized via the microcontroller. All timing-critical processes, i.e. the frequency sweep and the simultaneous signal acquisition, digitalization and processing (mostly the digital lock-in detection) are controlled by the FPGA.

VI. Measurements

A. VCO characteristics

The tuning characteristics of the detector ASIC where characterized with both VCOs embedded in their corresponding PLLs by sweeping the LO reference signal for different values of the ESR VCO biasing current I_{bias}. The reference signal of the offset PLL was kept constant, resulting in the ESR VCO frequency to follow the LO VCO with a constant offset. During the sweep the voltages $V_{\text{t,1,LO}}$ and $V_{\text{t,1,ESR}}$ where monitored and the results are plotted in Fig. 9. From the linear fit of the ESR VCO tuning characteristic, we calculated a gain of $K_{\text{V,1,ESR}} = 0.83\,\frac{\text{GHz}}{\text{V}}$ for $I_{\text{bias}} = 2.9\,\text{mA}$.

The second input port of the LO VCO $V_{\text{t,2,LO}}$ has not been characterized since it is not used for the cwESR experiments presented in this paper. To extract the VCO gain $K_{\text{V,2,ESR}}$ of the modulating port, we swept the voltage $V_{\text{t,2,ESR}}$ at a slow rate such that the offset PLL remains locked at all measurement points. Then, by measuring the tuning voltage $V_{\text{t,1,ESR}}$ and using the tuning sensitivity $K_{\text{V,1,ESR}}$ that has been measured previously, one can deduce the tuning sensitivity $K_{\text{V,2,ESR}}$. In this way, we measured a VCO gain for the modulation tuning port of $K_{\text{V,2,ESR}} = 34.4\,\frac{\text{MHz}}{\text{V}}$.

B. ESR measurements

We conducted various ESR experiments with the stable free radicals DPPH and BDPA to test the performance of the spectrometer. Here, as a first test, we measured the limit of detection (LOD) of the spectrometer, i. e. the minimum number of spins which can be detected with an SNR of 3 in 1 s of measurement time. To this end, we used a small grain of DPPH and measured its spectrum at a field of $B_0 = 452\,\text{mT}$ using different frequency modulation amplitudes. The resulting spectra together with the relevant experimental parameters are shown in Fig. 10. The corresponding measured LOD is $N_{\text{min}} = 1.7 \times 10^9\,\frac{\text{spins}}{\text{G}\sqrt{\text{Hz}}}$.

In a second experiment, we simultaneously placed the two different materials BDPA and DPPH, which display slightly

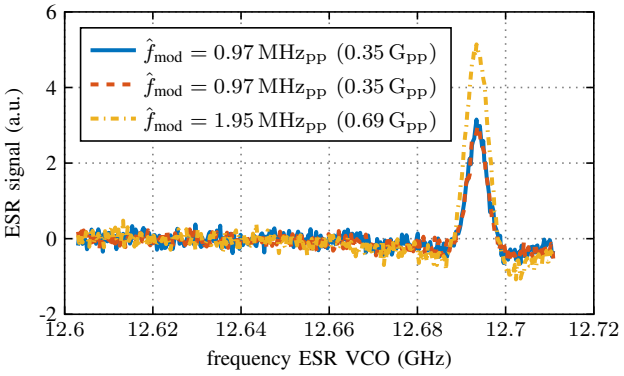

Fig. 10. Single shot ESR spectrum of a small grain of DPPH for different modulation amplitudes. Experimental parameters: $B_0 = 452\,\mathrm{mT}$, offset reference frequency 250 MHz, modulation frequency $f_{\mathrm{mod}} = 100\,\mathrm{kHz}$ and LIA time constant $T_{\mathrm{s}} = 1\,\mathrm{ms}$. Calculated limit of detections for the three different modulation amplitudes: $N_{\mathrm{min}} = 2.9 \times 10^9$, 2.4×10^9, 1.7×10^9 $\frac{\mathrm{spins}}{\mathrm{G}\sqrt{\mathrm{Hz}}}$

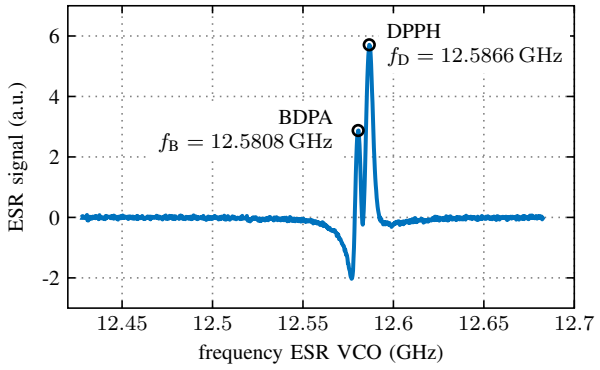

Fig. 11. ESR spectrum of a small grain of DPPH and a small crystal of BDPA jointly placed on the detection coil. Experimental parameters: four averages, $B_0 = 448\,\mathrm{mT}$, offset reference frequency 203 MHz, modulation frequency $f_{\mathrm{mod}} = 100\,\mathrm{kHz}$, $\hat{f}_{\mathrm{mod}} = 2.6\,\mathrm{MHz_{pp}}$ ($B_{\mathrm{mod,equiv}} = 0.93\,\mathrm{G_{pp}}$) and LIA time constant $T_{\mathrm{s}} = 1\,\mathrm{ms}$.

different g-factors of $g_{\mathrm{B}} = 2.00264$ [16] and $g_{\mathrm{D}} = 2.0036$ [17], on top of the detection coil. The corresponding spectrum is shown in Fig. 11. The extracted resonance frequencies f_{B} and f_{D} are annotated in the figure. Using the resonance frequencies measured in the spectrum and using the known B_0 value, one can extract g-factors of 2.0064 and 2.0073 for the two materials, which displays an error of only $0.18\,\%$ compared to the literature values. The residual error can be mostly attributed to uncertainties in the measurement of the B_0 field, which was carried out using a Hall probe near the chip and residual temperature fluctuations. The fact that the error in the g-factor determination corresponds to a pure offset can be seen by looking at the ratio of the two measured g-factors. Here, the ratio of f_{B} and f_{D} precisely corresponds to that of g_{B} and g_{D} with an error only around 1×10^{-5}, which corresponds to the relative frequency resolution of the conducted sweep which is around 2×10^{-5}.

VII. Conclusion

In this paper, we have presented an improved architecture for VCO-based ESR experiments that mitigates most of the tradeoffs commonly encountered in VCO-based ESR experiments. A second on-chip VCO removes the need for an on-chip frequency division, thereby relaxing the burden on the subsequent FM demodulator. Splitting the ESR detector's varactor into two separate devices provides near-optimal conditions both for wide frequency sweeps and precisely defined FM modulation signals. Finally, all on-chip VCOs are embedded into PLLs with external references, rendering their oscillation frequencies immune against PVT variations. Measured ESR results from a prototype realization demonstrate the excellent performance of the proposed architecture and its suitability for the realization of future portable point-of-care ESR spectrometers. As next steps, we will improve the resolution of the B_0 measurement by embedding one of our single chip NMR magnetometers [18] into our spectrometer.

Acknowledgment

This work was sponsored by the DFG within SPP1601 and under grant AN 984/5-1.

References

[1] M. J. Lawless, A. Shimshi, T. F. Cunningham, M. N. Kinde, P. Tang, and S. Saxena, "Analysis of nitroxide-based distance measurements in cell extracts and in cells by pulsed esr spectroscopy," *ChemPhysChem*, vol. 18, no. 12, pp. 1653–1660, 2017. [Online]. Available: https://onlinelibrary.wiley.com/doi/abs/10.1002/cphc.201700115

[2] Y. Yang, F. Yang, Y. Gong, J. Chen, D. Goldfarb, and X. Su, "A reactive, rigid gdiii labeling tag for in-cell epr distance measurements in proteins," *Angewandte Chemie*, vol. 129, no. 11, pp. 2960–2964, 2017. [Online]. Available: https://onlinelibrary.wiley.com/doi/abs/10.1002/ange.201611051

[3] P. Poprac, K. Jomova, M. Simunkova, V. Kollar, C. J. Rhodes, and M. Valko, "Targeting free radicals in oxidative stress-related human diseases," *Trends in Pharmacological Sciences*, vol. 38, no. 7, pp. 592 – 607, 2017. [Online]. Available: http://www.sciencedirect.com/science/article/pii/S0165614717300974

[4] C. L. Hawkins and M. J. Davies, "Detection and characterisation of radicals in biological materials using epr methodology," *Biochimica et Biophysica Acta (BBA) - General Subjects*, vol. 1840, no. 2, pp. 708 – 721, 2014, current methods to study reactive oxygen species - pros and cons. [Online]. Available: http://www.sciencedirect.com/science/article/pii/S0304416513001281

[5] W. He, Y. Liu, W. G. Wamer, and J.-J. Yin, "Electron spin resonance spectroscopy for the study of nanomaterial-mediated generation of reactive oxygen species," *Journal of Food and Drug Analysis*, vol. 22, no. 1, pp. 49 – 63, 2014, nanomaterials - Toxicology and Medical Applications. [Online]. Available: http://www.sciencedirect.com/science/article/pii/S1021949814000052

[6] S. De Wolf, C. Ballif, and M. Kondo, "Kinetics of a-si:h bulk defect and a-si:h/c-si interface-state reduction," *Phys. Rev. B*, vol. 85, p. 113302, Mar 2012. [Online]. Available: https://link.aps.org/doi/10.1103/PhysRevB.85.113302

[7] J. Handwerker, B. Schlecker, M. Ortmanns, and J. Anders, "Integrated circuit technology for next generation point-of-care spectroscopy applications," *IEEE Communications Magazine*, vol. 55, no. 10, pp. 143–151, 10 2017.

[8] D. Ha, J. Paulsen, N. Sun, Y.-Q. Song, and D. Ham, "Scalable nmr spectroscopy with semiconductor chips," *Proceedings of the National Academy of Sciences*, vol. 111, no. 33, pp. 11 955–11 960, 2014. [Online]. Available: http://www.pnas.org/content/111/33/11955

[9] J. Handwerker, B. Schlecker, U. Wachter, P. Radermacher, M. Ortmanns, and J. Anders, "A 14ghz battery-operated point-of-care esr spectrometer based on a 0.13µm cmos asic," in *2016 IEEE Int. Solid-State Circuits Conference (ISSCC)*, Jan 2016, pp. 476–477.

[10] A. Chu, B. Schlecker, J. Handwerker, S. Künstner, M. Ortmanns, K. Lips, and J. Anders, "Vco-based esr-on-a-chip as a tool for low-cost, high-sensitivity food quality control," in *2017 IEEE Biomedical Circuits and Systems Conference (BioCAS)*, 10 2017, pp. 1–4.

[11] B. Schlecker, A. Chu, J. Handwerker, S. Künstner, M. Ortmanns, K. Lips, and J. Anders, "Vco-based esr-on-a-chip as a tool for low-cost, high-sensitivity point-of-care diagnostics," in *2017 IEEE SENSORS*, 10 2017, pp. 1–3.

[12] K. Kyamakya, W. Mathis, R. Stoop, J. Chedjou, and Z. Li, *Recent Advances in Nonlinear Dynamics and Synchronization: With Selected Applications in Electrical Engineering, Neurocomputing, and Transportation*, ser. Studies in Systems, Decision and Control. Springer International Publishing, 2017. [Online]. Available: https://books.google.de/books?id=rDkuDwAAQBAJ

[13] J. Anders and M. Ortmanns, "Frequency noise of cmos lc tank oscillators operating in weak inversion," in *2013 European Conference on Circuit Theory and Design (ECCTD)*, Sept 2013, pp. 1–4.

[14] J. Anders, M. Ortmanns, and G. Boero, "Frequency noise in current-starved cmos lc tank oscillators," in *NDES 2012; Nonlinear Dynamics of Electronic Systems*, 07 2012, pp. 1–4.

[15] G. Gualco, J. Anders, A. Sienkiewicz, S. Alberti, L. Forró, and G. Boero, "Cryogenic single-chip electron spin resonance detector," *Journal of Magnetic Resonance*, vol. 247, pp. 96 – 103, 2014. [Online]. Available: http://www.sciencedirect.com/science/article/pii/S109078071400233X

[16] E. L. Dane, T. Maly, G. T. Debelouchina, R. G. Griffin, and T. M. Swager, "Synthesis of a bdpa-tempo biradical," *Organic Letters*, vol. 11, no. 9, pp. 1871–1874, 2009, pMID: 19331359. [Online]. Available: https://doi.org/10.1021/ol9001575

[17] J. Krzystek, A. Sienkiewicz, L. Pardi, and L. Brunel, "Dpph as a standard for high-field epr," *Journal of Magnetic Resonance*, vol. 125, no. 1, pp. 207 – 211, 1997. [Online]. Available: http://www.sciencedirect.com/science/article/pii/S1090780796910988

[18] J. Handwerker, M. Eder, M. Tibiletti, V. Rasche, K. Scheffler, J. Becker, M. Ortmanns, and J. Anders, "An array of fully-integrated quadrature tx/rx nmr field probes for mri trajectory mapping," in *ESSCIRC Conference 2016: 42nd European Solid-State Circuits Conference*, 09 2016, pp. 217–220.